Journal of Organometallic Chemistry xxx (xxxx) 121983

Contents lists available at ScienceDirect

Journal of Organometallic Chemistry

journal homepage: www.elsevier.com/locate/jorganchem

Effect of chirality and redox potentials on the cytotoxicity of new ferrocene functionalized chiral tertiary amines

Chirag J. Savani [a], Dushyanth R. Vennapu [b], Hetal Roy [c], Vinay K. Singh [a,*]

[a] Department of Chemistry, Faculty of Science, The M. S. University of Baroda, Vadodara, 390002, India
[b] Department of Pharmaceutical Chemistry, KLE University College of Pharmacy, Belagavi, Karnataka, 590010, India
[c] Department of Zoology, Faculty of Science, The M. S. University of Baroda, Vadodara, 390002, India

ARTICLE INFO

Article history:
Received 15 May 2021
Received in revised form 23 June 2021
Accepted 10 July 2021

Keywords:
Chirality
Ferrocene bearing tertiary amines
Anticancer
Molecular docking
DFT
Electrochemistry
Chiral tertiary amines
SCXRD
Cyclic voltammetry
TGA/DTA
Photophysical
Cytotoxicity

ABSTRACT

Optically pure enantiomeric pair viz. ferrocene functionalized chiral tertiary amines S,S-(-)-1 and R,R-(+)-2 have been synthesized from ferrocenylmethylamine to probe the influence of chirality and the redox potential on their anti-proliferative activity. Compounds were characterized by microanalysis, HPLC, ^{1}H, ^{13}C NMR, UV-visible, fluorescence, FTIR, thermogravimetric and crystallographic techniques. The single crystal X-ray diffraction (SCXRD) study revealed that the molecules of 1 holding S,S-chirality at benzylic carbons forms a fascinating M-helix while 2 holding R,R-chirality at benzylic carbons forms P-helix by involving intra- and intermolecular H-bonding interactions as verified by Hirshfeld surface analysis. Chirality-related influence was observed on the antiproliferative activity of enantiomeric pair and at the supramolecular level. For instance, enantiomer R,R-(+)-2 is found to be highly active against all the investigated human carcinoma cell lines MCF 7, IMR 32, HepG2, and immortal L132 cell lines. In particular, R,R-(+)-2 exhibited more than 10 folds better antiproliferation (IC_{50}: 6.35 ± 0.19 μM) than other enantiomer S,S-(-)-1 (IC_{50}: 65.96 ± 0.12 μM) and four folds better activity than highly successful anticancer drug, cisplatin (IC_{50}: 24.3 ± 1.7 μM) against Hep G2 cell line. The electrochemical, DFT calculations and molecular docking study have been performed to justify the experimental outcomes.

© 2021

1. Introduction

The interest in developing novel organic,[1] inorganic [2] and organometallic [3] compounds as antitumor agents has been continued because cancer has become the second leading cause of death globally and this burden continues to increase day by day. An estimated 9.6 million deaths have been recorded due to cancer in the year 2018 [4]. This has created a growing interest in developing chiral metal-based drugs with their unique properties and potential selectivity toward nucleic acids and protein based chiral biomolecules [5]. Chirality has become an important tool in modern drug development because one of the enantiomers may be beneficial, while the other may be harmful and thus their therapeutic activity can differ severely in terms of toxicity and pharmacokinetics [6]. For instance, a Pt(II) antineoplastic drug in clinical use "oxaliplatin" contains the chiral ligand (R, R)-cyclohexane-1,2-diamine showed more biological activity and chemical reactivity than its enantiomer containing the ligand (S, S)-cyclohexane-1, 2-diamine [7]. There has been significant interest in the research on chiral metal-based compounds for anticancer application [8]. A ferrocene containing compounds have been emerged as a novel class of anticancer drug. To achieve better medicinal properties, biologically relevant chemotherapeutic agents or groups have been methodically attached into the cyclopentadienyl ring of ferrocene, [9] which may offer chirality into the molecule [10]. For instance, Kater et al. have reported enantiomerically pure ferrocene–amino acid derivative showing a pronounced anticancer activity against leukemia and lymphoma cancer cell lines, which has overcome multiple drug resistance [11].

Recently, we have tested the scope of a new series of analogous achiral tertiary amines for apoptotic potentials against various human cancer cell lines in low μM concentration [9a]. The apoptotic regulatory influence of various substituents of amidic nitrogen in these compounds on TNFα inhibition discloses an optimal substitution of N-benzyl group [9a]. A remarkable increase in anticancer activity of analogous achiral tertiary amines holding benzyl substituted amidic nucleus has encouraged us to carry out further structural modification by introducing chi-

* Corresponding author.
E-mail address: vinay.singh-chem@msubaroda.ac.in (V.K. Singh).

https://doi.org/10.1016/j.jorganchem.2021.121983
0022-328/© 2021

UNCORRECTED PROOF

rality at the benzylic carbon to achieve chiral tertiary amine enantiomeric pair S,S-(-)-1 and R,R-(+)-2. Since DNA is chiral by itself and by anticipating our enantiomeric pair to operate by a pathway similar to that of chiral-drug, [7a] we have selected to probe the influence of chirality on anticancer properties.

In this work, we have synthesized two optically pure enantiomeric pair viz. ferrocene functionalized chiral tertiary amines S,S-(-)-1 and R,R-(+)-2 from ferrocenylmethylamine and these were characterized by microanalysis, ^{1}H, ^{13}C NMR, UV-visible, fluorescence, FTIR, thermogravimetric and crystallographic techniques. Chirality-dependent formation of left- (M type) and right- (P type) handed helices, confirmed by SCXRD, and its dependency on the antiproliferative activity of enantiomeric pair was verified by MTT assay. The results on anticancer potential of enantiomers have been well supported by molecular docking, DFT and electrochemical study. The synthesized enantiomer R,R-(+)-2 contained an optimal anticancer potential in low micro molar concentration. This allows us to probe the chirality-influence on anticancer potentials of enantiomers and their secondary interactions with the 2AZ5 and 1TNF proteins.

2. Results and discussion

2.1. Synthesis and characterization

The optically pure ferrocene functionalized chiral tertiary amines bearing pendant amidic groups S,S-(-)-1 and R,R-(+)-2 as shown in Scheme 1 were conveniently synthesized from α-iodoamide precursors IA1-IA5 and ferrocenylmethyamine. An analogous compound 3 was reproduced [9a] and its molecular structure was determined unambiguously for comparison purpose. After column chromatography the products were obtained as yellow powders in 87–90% isolated yield. These compounds are soluble in common organic solvents and stable in the solution over days. The composition and purity of these compounds

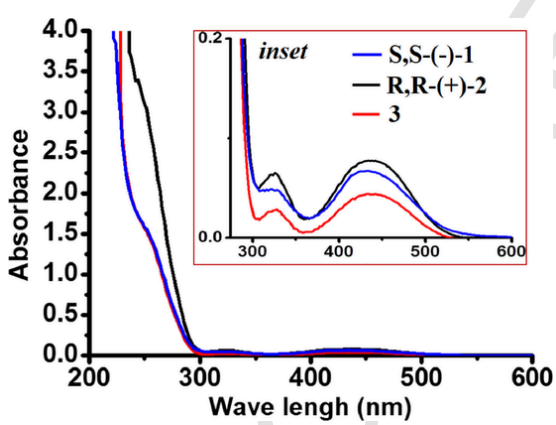

Fig. 1. UV-visible absorption spectrum of the compounds under investigation at room temperature in 10^{-5} M CH_3CN.

Table 1
UV-visible and fluorescence bands for compounds under investigation.

Entry	Selected IR Bands (KBr, cm^{-1})		UV-Visible data (10^{-5} CH_3CN)λ_{max} nm (ε L Mol^{-1} cm^{-1})	Fluorescence spectrum data (10^{-5} M CH_3CN)	
	υ(NH)	υ(CO)		λ_{ex} (nm)	λ_{em} nm (Intensity)
1	3313, 3240	1666, 1639	253 (14787) π→ π*325 (6469) n→ π* 435(7254) charge transfer	435	491 (40) CT
2	3397, 3236	1658, 1639	243 (33613) π→ π* 325(2756) n→ π* 437(4628) charge transfer	435	491 (42) CT
3	3448, 3313	1670, 1639	249 (16678) π→ π* 326 (4770) n→ π* 438(7737) charge transfer	435	490 (35) CT

were confirmed by elemental analyses, HPLC, NMR and IR spectroscopy.

The UV-visible spectrum of all compounds shown in Fig. 1 gives three absorption bands in the region of 243–253 nm, 300–400 nm and 400–500 nm. In analogy with the earlier report [9c], these transitions are assigned to intra-ligand π→ π*, n–π* symmetry-allowed transition of the type 3d-MO* and to a forbidden d–d transition localized on the iron metal center respectively."

All the compounds fluoresce in the visible region (Table 1, Fig. S10) with a concomitant Stokes shift of ~55 nm wherein highest fluorescence intensity band was observed for enantiomer R,R-(+)-2. Enantiomers S,S-(-)-1 and R,R-(+)-2 and compound 3 showed an endothermic peak at 141.1 °C, 142.3 °C and 142.8 °C, respectively in DTA curves (Fig. S12), without any mass loss on DTG curves, and these peaks attributes to the melting point of the compounds. Notably, TGA curves of these compounds show one-step decomposition in the 250–550 °C temperature range with weight loss of 61.0, 75.8 and 70.8 %, respectively, however we could not observe a stable residual mass on TG curve and weight loss continues till 550 °C.

Notably, compounds show two different CO stretching frequencies in 1658–1639 cm^{-1} region (Table 1, Fig. S7- Fig. S9) due to the involvement of both CO in diverse H-bonding interactions as verified by SCXRD study.

2.2. X-ray crystallographic study

Solid samples crystallize in monoclinic $P2_1$, S,S-(-)-1 and R,R-(+)-2 and orthorhombic 3, centrosymmetric space groups. The X-ray crystal structure shows two complete molecules in their asymmetric units, except 3, which contains one complete molecule in its asymmetric unit. The ORTEP view at 50% probability for these compounds is shown in Fig. 2. Details about data collection, refinement, and structure solution are recorded in Table S1 and selected geometrical parameters are tabulated in Table 2. The structural parameters are found to be in the normal range [9a], except, the N-C bond lengths and C-N-C bond angles associated with tertiary amino groups of compounds S,S-(-)-1 and R,R-(+)-2. Notably, the average N-C bond lengths associated with tertiary amino groups in enantiomeric pair S,S-(-)-1 and R,R-(+)-2 (ca 1.44 Å) is slightly shorter than the corresponding average N-C bond lengths of

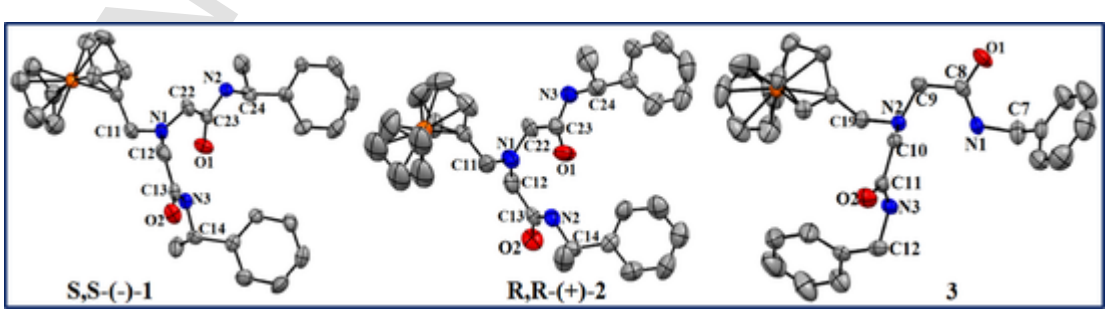

Fig. 2. The ORTEP diagram with partial atom numbering showing 50% probability ellipsoid; (hydrogen atoms are omitted for clarity).

Table 2
Selected bond length and bond angles of S,S-(-)-1, R,R-(+)-2 and 3.

Selected Bond Lengths(Å)	Selected Bond angles(°)
S,S-(-)-1	
N_3-C_{14} = 1.441(9); N_3-C_{13} = 1.352(8); O_2-C_{13} = 1.235(9); C12-C_{13} = 1.534 (11); N_1-C_{12} = 1.409(10); N_1-C_{11} = 1.474(10); N_1-C_{22} = 1.395(9); C_{22}-C_{23} = 1.535(9); O_1-C_{23} = 1.230(8); N_2-C_{23} = 1.340(9); N_2-C_{24} = 1.478(8)	O_1-C_{23}-N_2 = 124.5(6); O_1-C_{23}-C_{22} = 121.7(6); N_2-C_{23}-C_{22} = 113.8(6); O_2-C_{13}-C_{12} = 121.2(6); O_2-C_{13}-N_3 = 123.2(7); N_3-C_{13}-C_{12} = 115.6(7); C_{11}-N_1-C_{22} = 117.5(6); C_{11}-N_1-C_{12} = 121.3(6); C_{12}-N_1-C_{22} = 121.1(6).
R,R-(+)-2	
N_2-C_{13} = 1.326(7); N_2-C_{14} = 1.458(9); C_{12}-C_{13} = 1.523(11); O_2-C_{13} = 1.228 (8); N_1-C_{11} = 1.464(9); N_1-C_{12} = 1.425 (10); N_1-C_{22} = 1.411(8); C_{22}-C_{23} = 1.509(9); O_1-C_{23} = 1.230(8); N_3-C_{23} = 1.320(8); N_3-C_{24} = 1.472(8).	O_1-C_{23}-N_3 = 124.6(6); O_1-C_{23}-C_{22} = 121.0(6); N_3-C_{23}-C_{22} = 114.3(6); O_2-C_{13}-C_{12} = 120.3(5); O_2-C_{13}-N_2 = 123.5(7); N_2-C_{13}-C_{12} = 116.1(6); C_{11}-N_1-C_{22} = 117.1(7); C_{11}-N_1-C_{12} = 122.2(6); C_{12}-N_1-C_{22} = 120.6(6).
3	
N_1-C_7 = 1.454(4); N_1-C_8 = 1.340(4); C_8-C_9 = 1.515(4); O_1-C_8 = 1.229(3); N_2-C_9 = 1.463(4); N_2-C_{19} = 1.482(3); N_2-C_{10} = 1.458(3); C_{10}-C_{11} = 1.513(4); O_2-C_{11} = 1.235(3); N_3-C_{11} = 1.332(4); C_{12}-N_3 = 1.457(4).	O_1-C_8-N_1 = 123.0(3); O_1-C_8-C_9 = 120.1 (3); N_1-C_8-C_9 = 116.8(3); O_2-C_{11}-C_{10} = 119.4(3); O_2-C_{11}-N_3 = 123.2(3); N_3-C_{11}-C_{10} = 117.4(2); C_9-N_2-C_{10} = 111.6(2); C_9-N_2-C_{19} = 111.9(2); C_{10}-N_2-C_{19} = 112.7(2).

1.47 Å in analogous compound 3. Further, the average C-N-C bond angles in S,S-(-)-1 and R,R-(+)-2 (ca 119.9°) deviates from the normal range and found to be significantly larger than the corresponding average C-N-C bond angle of 112.1° in 3. The experimentally obtained structural parameters are comparable with the similar parameters obtained theoretically (Table S3, ESI) by DFT calculations.

Notably, two molecules present in the asymmetric unit cell of enantiomeric pair S,S-(-)-1 and R,R-(+)-2 adopt different alignments. For instance, in S,S-(-)-1, ferrocenyl groups are found to be far from each other (Fig. S13) whereas they are in the close vicinity in R,R-(+)-2 (Fig. S14). Besides, the dihedral angles formed by two phenyl ring planes of first asymmetric molecule in S,S-(-)-1 (24.03°) and R,R-(+)-2 (23.61°) deviates largely from the similar angles in the second asymmetric molecule of S,S-(-)-1 (1.99°) and R,R-(+)-2 (1.70°) (Fig. S14). Nearly orthogonal alignment of two phenyl rings can be visualized in the analogous asymmetric molecule 3 (Fig. S15). Thus, due to different conformational modes adopted by amidic groups in both the asymmetric molecules of enantiomeric pair S,S-(-)-1 and R,R-(+)-2, they are involved in varied supramolecular packings. For instance, first asymmetric molecule of S,S-(-)-1 is primarily engaged in the formation of intra- and intermolecular hydrogen bonding interaction involving N_2H_2…O_1 (2.041 Å, intra-molecular) and donor-acceptor N_3H_3…O_2 (2.024 Å, intermolecular) H-bonding interactions. This leads to a fascinating 1D helical (M-type, left-handed) supramolecular arrangement of molecules with helical pitch of 12.085 Å as shown in Fig. 3. Interestingly, first asymmetric molecule of R,R-(+)-2 with similar intermolecular contacts vis. N_2H_2…O_1 (2.094 Å, intra-molecular) and donor-acceptor N_3H_3…O_2 (2.050 Å, intermolecular) H-bonding contacts lead to the formation of opposite 1D helical (P-type, right-handed) supramolecular structure with helical pitch of 12.177 Å (Fig. 4). Lack of intra-molecular H-bonding interactions in the second asymmetric molecule of enantiomeric pair S,S-(-)-1 and R,R-(+)-2, leading to 1D zig-zag molecular arrangements through donor-acceptor N_5H_5…O_4 (2.013 Å) and N_6H_6…O_4 (2.042 Å) intermolecular H-bonding interactions as shown in Fig. S16 and Fig. S17. The variations in the stereochemical environment of various groups in the analogous compound 3 resulted into linear 1D sheet through N_3H_3…O_2 (2.110 Å) intermolecular H-bonding interactions (Fig. 5).

Helicity in supramolecular constructions apparently induced by conformation limits of molecules, inter, intra-molecular hydrogen bonds, or coordination to metal ions. Reportedly, a majority of helical molecular assemblies in the crystalline phase are based on the use of achiral building blocks [12]. Thus, chirality induced formation of left-handed (M-type) and right-handed (P-type) helices and their influences on the anti-proliferative activity (discussed later) of the enantiomers (discussed later) adds merit to this work.

Hirshfeld surface analysis [13] was performed to quantify these noncovalent intermolecular interactions such as H-bonding and π-forces (Fig. S18). The relative contributions of the intermolecular interactions to the Hirshfeld surface for the compounds S,S-(-)-1, R,R-(+)-2 and 3 [%] are shown in Table S2. For instance, S,S-(-)-1 exhibits; H/H

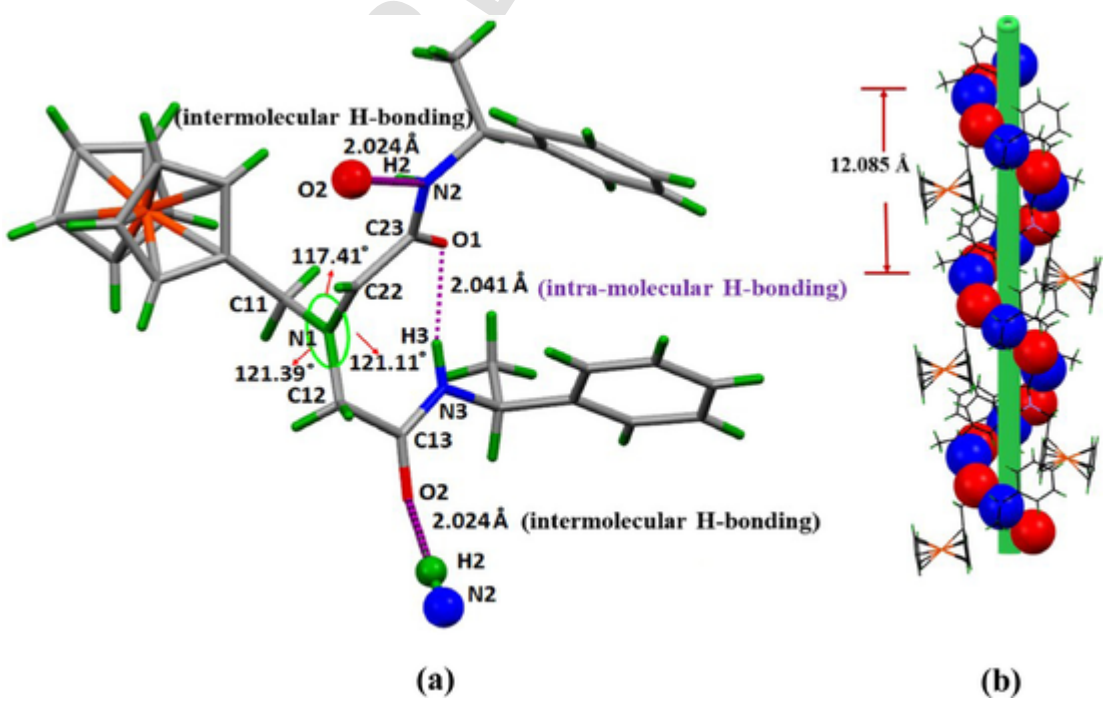

Fig. 3. First asymmetric molecule of S,S-(-)-1 showing propensity to form (a) intra- and intermolecular H-bonding, (b) S,S-(-)-1 forming fascinating 1D M-helix through NH-O (inter) and NH-O (intra) with helical pitch of 12.085 Å.

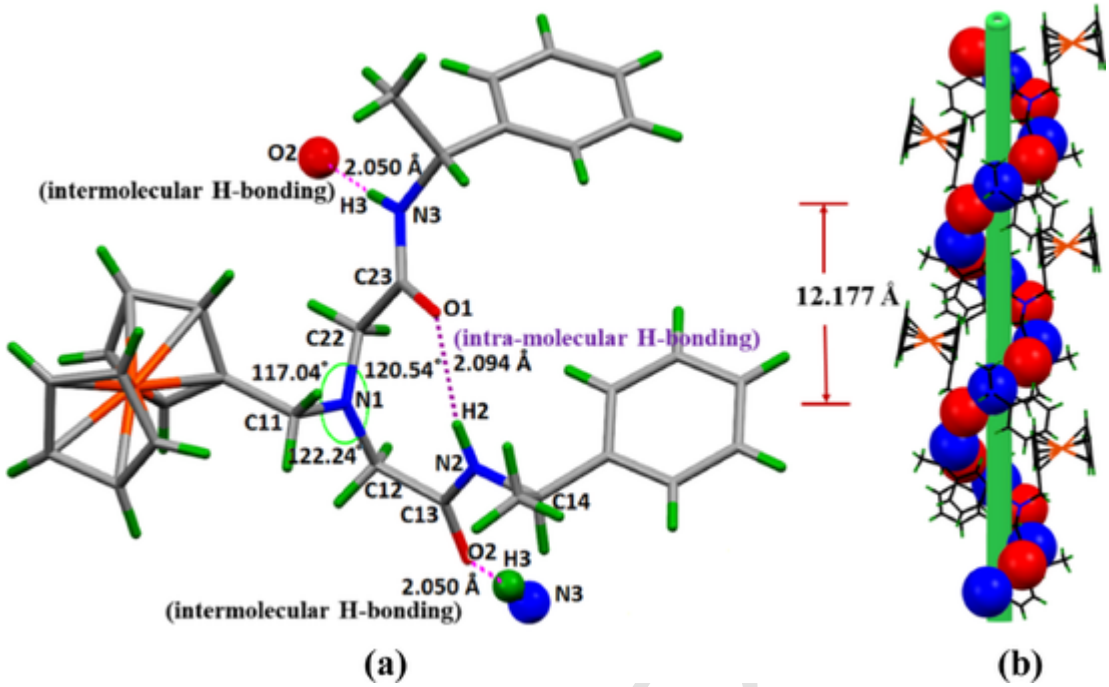

Fig. 4. First asymmetric molecule of R,R-(+)-2 showing propensity to form (a) intra- and intermolecular H-bonding, (b) R,R-(+)-2 forming fascinating 1D P-helix through NH-O (inter) and NH-O (intra) with helical pitch of 12.177 Å.

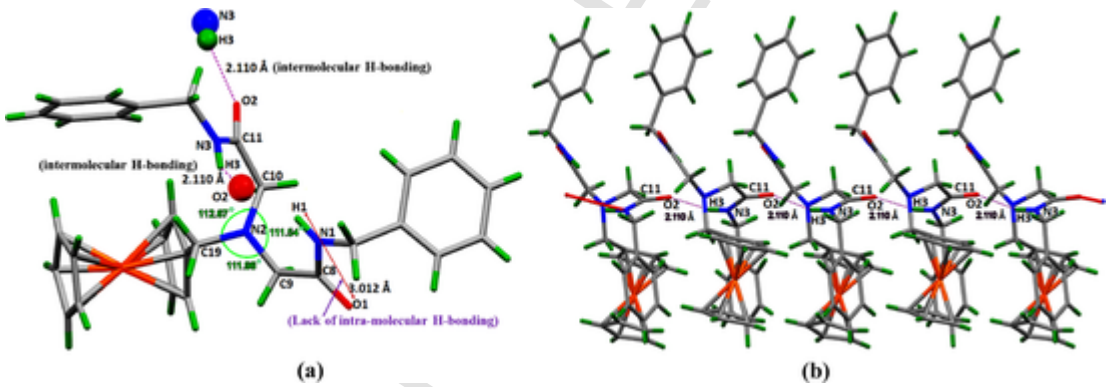

Fig. 5. Asymmetric molecule of 3 showing propensity to form (a) only intermolecular H-bonding and (b) arranges the molecules of 3 along b-axis linearly into a 1D sheet like architecture.

(67.3%), C/H (23.3%), O/H (8.7%), R,R-(+)-2 exhibits; H/H (64.0%), C/H (25.2%), O/H (9.6%) while achiral molecules of 3 exhibits; H/H (61.9%), C/H (24.2%), O/H (12.2%) weak intermolecular interactions. Apparently, this shows the ability of these molecules to inhibit cell growth by offering secondary interaction in the biological system. In the mapping of electrostatic potential surface (Fig. S21), the occurrence of negative potential over the amide oxygen and positive potential is around the amide proton are mainly responsible for the existence of donor-acceptor intermolecular contacts involving amidic groups in S,S-(-)-1, R,R-(+)-2 and 3.

2.3. Inhibitory activity and structure activity relationships (SAR)

Ferrocene is involved in the generation of reactive oxygen species (ROS) within the cells, improvement of biological activity, overcome resistance barriers, lipophilic character, redox activity, and enabling easier passage through cell membranes [3b,14]. Moreover, the incorporation of amino groups into the molecular skeleton benefits in an active transport process through the formation of organic cation transporter and thereby improves the biological activity [15]. Therapeutic activities of many drugs available in the market viz. penicillin G, mociobemide, acetazolamide, arimethobenzamide, etc. have been connected with amide linkage in the nucleus [16]. In the light of these observations, we have recently tested the apoptotic potentials of ferrocene functionalized achiral tertiary amines against several human cancer cell lines MCF 7, IMR 32, L132 and Hep G2 in low μM concentration [9a]. A remarkable increase in anticancer activity of these compounds holding N-benzyl substitution at the amidic nitrogen encouraged us to introduce chirality at the N-benzylic carbon to probe the chirality-related influence on the antiproliferative activity of enantiomeric pair S,S-(-)-1 and R,R-(+)-2.

One of our enantiomer R,R-(+)-2 (optical rotation = +89°) displayed enhanced cytotoxic activity against all the investigated cell lines (MCF 7, IMR 32, HepG2, and immortal L132) compared to the other S,S-(-)-1 (optical ration = -87°) as shown in Table 3, Fig. 6.

The IC_{50} values of synthesized inhibitors were found to be most effective on HepG2 amongst all the investigated cell line cells. In particular, R,R-(+)-2 exhibited more than 10 folds better cytotoxic activity (IC_{50}: 6.35 ± 0.19 μM) against human hepatoma cancer cells Hep G2 than S,S-(-)-1 (IC_{50}: 65.96 ± 0.12 μM) and four folds better activity than

Table 3
In vitro cytotoxicity on cell line after 24 hours of enantiomers S,S-(-)-1, R,R-(+)-2 and analogous achiral compound 3.

	Ligand	IC_{50} values (μM)[a]			
		MCF 7	IMR 32	L132	HepG2
1	S,S-(-)-1	63.91 ± 0.08	101.10 ± 0.12	97.98 ± 0.13	65.96 ± 0.12
2	R,R-(+)-2	48.16 ± 0.20	31.91 ± 0.08	11.08 ± 0.20	6.35 ± 0.19
3	3[b]	23.63 ± 0.12	52.11 ± 0.11	22.37 ± 0.13	7.25 ± 0.11
4	Cisplatin	32.41 ± 1.5	29.6 ± 1.26	21.4 ± 2.2	24.3 ± 1.7

[a]Values are represented as Mean ± SEM. [b] IC50 value retrieved from reference [9a].

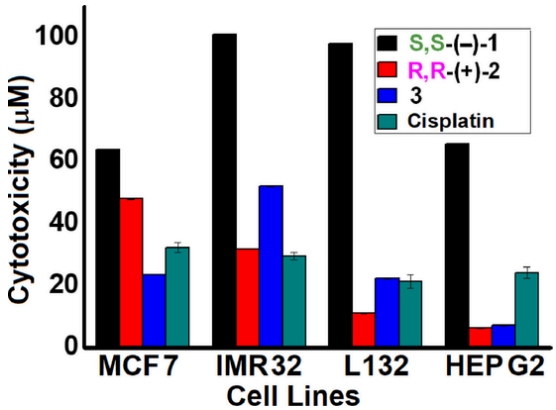

Fig. 6. Cytotoxicity (μM) of ferrocene functionalized enantiomers S,S-(-)-1, R,R-(+)-2 and analogous achiral compound 3.

highly successful anticancer drug, cisplatin (IC_{50}: 24.3 ± 1.7 μM). Further, this enantiomer R,R-(+)-2 showed better cytotoxic profile then the analogous achiral compound 3. Thus chirality-dependent formation of left- (M type) and right- (P type) handed helices and its influence on the antiproliferative activity of enantiomeric pair has been validated. The significant differences in antiproliferative activity of the enantiomeric pair may be arises due to differences in their helicity as well as in their helical pitches (vide supra).

The presence of R,R-chirality is found to be crucial for enhanced activity in the biological system. A strong anticancer potential of enantiomer R,R-(+)-2 has been well supported by molecular docking study (discussed later). Evidently, the introduction of R,R-chirality at both the N-benzylic groups in R,R-(+)-2 offering a great number of H-bonding interactions with 2AZ5 and TNFR1 proteins and thus providing stability to the R,R-(+)-2 inhibitor which apparently resulted into enhanced bioactivity. Moreover, mapping of electrostatic potential surface (Fig. S21) of R,R-(+)-2 inhibitor demonstrates that polar amide subunits are projected in such a way that it provides H-bond donor-acceptor sites to facilitate an effective H-bonding interactions with the protein molecules (discussed latter), leading to adequate cellular membrane transportation, [17] triggering an increased concentration at the active site.

2.4. Electrochemistry

The lower cytotoxic activity of hydroxyferrocifens against both hormone-independent (ER-) and hormone-dependent (ER+) cancer cells, compared to hydroxytamoxifen, arises from the in situ oxidation of Fe^{2+} to Fe^{3+} ions and thus cell death has been linked with the oxidation of ferrocene to ferrocenium cation. The ferrocenium group appears to play the role of an intramolecular electron acceptor in the in vitro cytotoxicity as evidenced by the transience of the electrochemically produced Fe^{3+} center in the presence of pyridine [18]. We have used electrochemistry further to establish the structure-activity relationship and the influence of redox potential of these compounds on their cytotoxic activity.

The voltammograms (Fig. 7) clearly reveals the significant differences in the electrochemical stability of the enantiomers. The exact reason for the electrochemical recognition of these enantiomers is not known, however this may be apparently arising due to the involvement of distinct H- bonding interactions leading to the formation of left- and right-handed helices by the enantiomers with different helical pitches (vide supra).

The observed cytotoxicity of the enantiomers S,S-(-)-1, R,R-(+)-2 and analogous achiral compound 3 (Fig. 6, Table 3) appeared to follow the opposite order to their half-cell potentials E1/2 (Fig. 7, Table 4). For instance, the IC_{50} followed the order R,R-(+)-2 > 3 Ni > S,S-(-)-1, while the $E_{1/2}$ followed R,R-(+)-2 < 3 < S,S-(-)-1 order against human hepatoma (HepG2) and neuroblastoma (IMR 32) cancer cell lines. Similar dependances of cytotoxicity on redox potentials have been observed earlier in a series of 2-arylidenebenzocycloalkanones, 1,3-diarylidene-2-tetralones, 3,5-bis-arylidene-4-piperidones and ferrocene pyrazole conjugates [19].

It may be anticipated that the biologically active enantiomer undergoes oxidative metabolism, which is enhanced by the easier oxidation of ferrocene. The redox active ferrocene moiety may be oxidized by the biological target and might serve as a transporter of the hole while the activated drug finds its way to reach to the target [18]. A small degree of coupling between the ferrocenium-centered radical with other radical species may lead to a relatively high energy transition state, which may stabilize the ferrocenium species on its path to the target [20].

2.5. Pharmacophoric interactions of S,S-(-)-1, R,R-(+)-2 and 3 with TNFα (PDB ID: 1TNF and 2AZ5)

Molecular docking for protein-ligand interactions have been performed to determine the binding mode of synthesized inhibitors S,S-(-)-1, R,R-(+)-2 and 3 with the active sites of TNFα (PDB ID: 1TNF and 2AZ5) protein. The molecular docking on to both the proteins showed complementary H-bonding and hydrophobic interaction with active

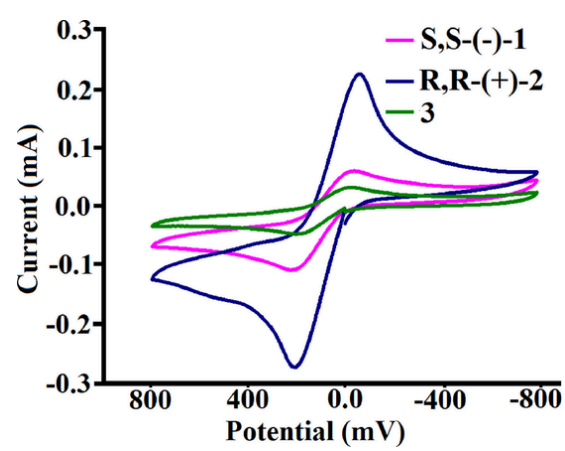

Fig. 7. Cyclic voltammograms of a 2.0 mM solution of the ferrocene functionalized chiral tertiary amines S,S-(-)-1 and R,R-(+)-2 and compound 3 in CH_3CN containing 0.2 M TBAP, glassy carbon (BAS) working electrode, Pt counter, Ag/AgCl reference electrode; CV: scan rate = 1000 mV s^{-1}.

Table 4
Electrochemical data for of the ferrocene functionalized chiral tertiary amines S,S-(-)-1 and R,R-(+)-2 and compound 3 at a scan rate of 1000 mVs^{-1}.

Entry	Compounds	Scan rate/ mVS^{-1}	E_{Pc} (mV)	E_{Pa} (mV)	$E_{1/2}$ (mV)	Ep(mV)
1	S,S-(-)-1	1000	-34	214	90	248
2	R,R-(+)-2	1000	-60	205	72.5	265
3	3	1000	-23	198	87.4	110

UNCORRECTED PROOF

site of the protein (Fig. S27-Fig. S32, ESI). The dock scores for each inhibitor with different poses have been represented in Table 5. The dock score clearly showed that inhibitor R,R-(+)-2 selectively bind to both the proteins with maximum number of H-bonding interactions than the other inhibitors i.e. the most potent enantiomer R,R-(+)-2 has prominent H-bonding interactions with both 2AZ5 (via Leu-120 and Gly-121) and 1TNF (via Lys-98, Tyr-119 and Ile-118) in addition to several hydrophobic interactions within 6A^0 space of receptor pocket (active site) with optimum dock scores. Although, inhibitor R,R-(+)-2 and 3 have shown the ability to interact with 1TNF through a common H-bonding site of Tyr-119, however bonding of inhibitor R,R-(+)-2 is found to be significantly stronger than 3 as shown in Fig. 8. Thus chirality-influence on ligand-protein interactions (Table 5) is consistent with the observed cytotoxicity of these inhibitors. It has been shown that derivatives of TNFα target effect on angiogenesis as well as reduced toxicity, as an antitumor agent in comparison to cisplatin, doxorubicin, paclitaxel and melphalan on some cancer such as lymphoma, breast cancer [21].

Pharmacokinetic profiling (computational prediction) of these compounds (ESI) revealed that all the molecules under investigation have optimum cell permeability are within the range (< 140 Å^2 and AlogP98 < 5) [23]. Drug-likeness prediction of investigated molecules has been ascertained by using radial plot of Flare Viewer (Fig. S24), radial plot using Swiss Adme (Fig. S25) and Molsoft (Fig. S26). All the molecules exhibited best fit with all the models and possesses lead-likeness characteristics.

Table 5
Non-bonding interactions within 6 Å of Active site 2AZ5 & 1TNF

Ligand	PDB	Hydrogen Bonding Interaction (within 6 Å)	Hydrophobic Interaction (within 6 Å)	Binding Energy Kcal/mol
S,S-(-)-1	2AZ5	-	TYR-59, Ile 155, LEU-57	-5.7
R,R-(+)-2	2AZ5	Leu-120 & Gly-121	Tyr 59, Tyr 119, Leu 57, Ile 155,	-6.5
3	2AZ5	-	Lue-57, Tyr 119, TYR-59, Leu 57, Val 123, Leu 157	-5.9
Co-Crystal	2AZ5	Tyr-59	Leu-57, Tyr-59, GLY-121, Tyr-119 & Le- 120	-7.0
S,S-(-)-1	1TNF	GLY-121	Lue-120, Pro-117, Ala96, Lys-98,Ile-118,Lue-94, Ala96	-5.9
R,R-(+)-2	1TNF	Lys-98, Tyr-119, Ile-118	Ala-96	-6.0
3	1TNF	Tyr-119 & Pro-117	Tyr-119,Lue-120, Ala96, Lys-98, Pro-117, Ile-118	-6.0

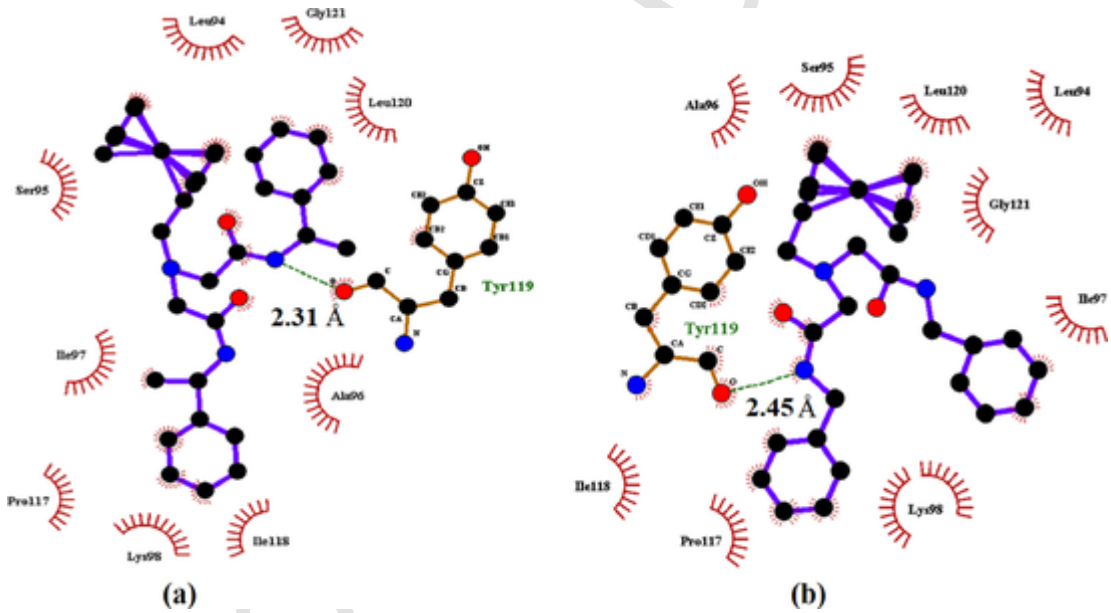

Fig. 8. Binding of R,R-(+)-2 and analogues compound 3 with TNFα receptor plotted using Ligplot+: multiple ligand-protein interaction diagrams [22].

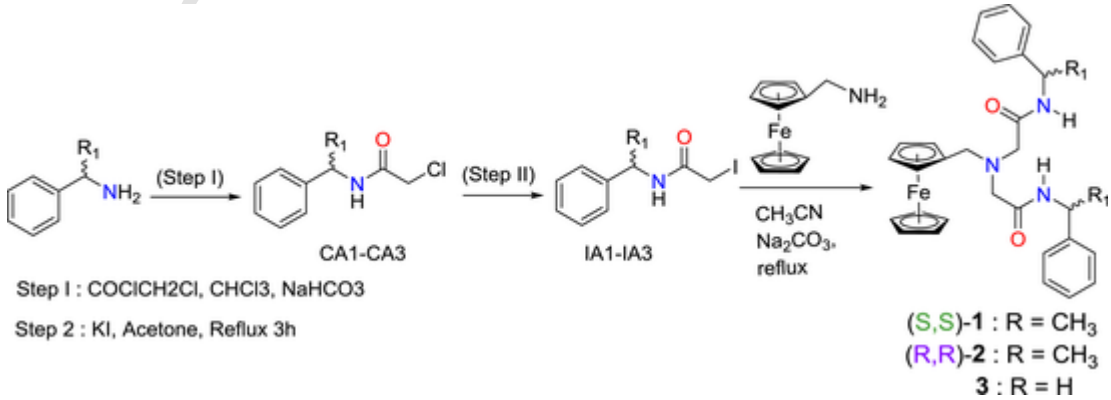

Scheme 1. Synthesis of 2,2'-(ferrocenylmethylazanediyl)bis(N-((S)-1-phenylethyl)acetamide) S,S-(-)-1, 2,2'-(ferrocenylmethylazanediyl)bis(N-((R)-1-phenylethyl) acetamide) R,R-(+)-2 and 2, 2'-(ferrocenylmethylazanediyl)-bis-(N-benzylamide) 3.

3. Conclusions

A remarkable increase in anticancer activity with benzyl swapped at the amidic nitrogen of analogous ferrocene functionalized achiral tertiary amines [9a] has encouraged us to introduce diverse chirality at the N-benzylic carbon and to probe their influence on photophysical, electrochemical, ligand-protein bonding efficacy and anticancer properties of ferrocene functionalized chiral tertiary amine enantiomers S,S-(-)-1 and R,R-(+)-2. The results showed that optically pure enantiomer R,R-(+)-2 forming the right-handed helical motif at supramolecular level, displayed stronger inhibition against all the investigated cell lines MCF 7, IMR 32, HepG2, and immortal L132 cell lines of human origin as compared to enantiomer S,S-(-)-1 and an analogues compound 3. The chirality in the molecules at the atomic level guiding the self-assembly at supramolecular level in a similar way as the proteins we observe in living organisms. Results suggest that a change in chirality changes the redox potential, fluorescence, ligand-protein bonding efficacy and the bio-activity of the molecules, considerably. For instance, the enantiomer R,R-(+)-2 with lowest half-electrode potential (E1/2) and prominent H-bonding interactions with 2AZ5 (through Leu-120 and Gly-121) and 1TNF (through Lys-98, Tyr-119 and Ile-118) showed many folds ca 10 folds better cytotoxicity (IC_{50}: 6.35 ± 0.19 μM) than other enantiomer S,S-(-)-1 (IC_{50}: 65.96 ± 0.12 μM) against Hep G2 cell line. The biological characterization of these compounds provides convincing sign to recommend that enantiomer R,R-(+)-2 has potentials for further development as anticancer agent with high efficacy against multiple cancer types.

4. Experimental section

Material and physical measurements. Ferrocenylmethylamine, α-chloroamide precursors (CA1-CA3), α-iodoamide precursors (IA1-IA3) and compound 3 were synthesized by a modified literature procedure [9a]. Syntheses using anhydrous solvents were carried out under Schlenk conditions. All the chemicals and solvents used in this work were of laboratory grade available at various commercial sources and used without further purification. Thin Layer Chromatography was performed on Merck 60 F254 aluminium coated plates. FT-IR (KBr pellets) spectra were recorded in the 4000–400 cm^{-1} range using a Perkin-Elmer FT-IR spectrometer. The NMR experiments were carried out on a Bruker AV-III 400 MHz spectrometer in $CDCl_3$ solvents as per the solubility and chemical shifts are reported in parts per million (ppm). UV-visible absorption spectra were recorded on a JASCO V-730 UV-visible spectrophotometer Fluorescence was recorded on JASCO make spectrofluorometer model FP-8200. TGA/DTA plots were obtained using SII TG/DTA 6300 in flowing N_2 with a heating rate of 10 °C min^{-1}. Electrochemical measurements were performed on a CH Instruments 600C potentiostat, using a glassy carbon as the working electrode, Ag/AgCl as the reference electrode and a Pt wire as the counter electrode. Voltammograms were recorded by using anhydrous solutions of the 2.0 mM ferrocene functionalized tertiary amines 1–3 in CH_3CN containing 0.2 M tetra-n-butylammoniumhexafluoro phosphate (TBAP) as supporting electrolyte.

Synthesis of 2,2'-(ferrocenylmethylazanediyl)bis(N-((S)-1-phenylethyl)acetamide) S,S-(-)-1, and 2,2'-(ferrocenylmethylazanediyl) bis(N-((R)-1-phenylethyl)acetamide) R,R-(+)-2.

(S)-2-iodo-N-(1-phenylethyl)acetamide (592 mg, 2.05 mmol) and (R)-2-iodo-N-(1-phenylethyl)acetamide (592 mg, 2.05 mmol) were added portion wise to the solution of aminomethylferrocene (215 mg, 1 mmol) in 25 ml of CH_3CN containing Na_2CO_3 (0.265 g, 2.5 mmol). The reaction mixture was reflux for 6 h. The progress of the reaction was monitored by thin layer chromatography. The reaction mixture was cooled at room temperature and solvent was removed under vacuum. Distilled water was added in the solid residue and the crude product was extracted by using dichloromethane. It was dried over Na_2SO_4 for 4 h and the solvent was removed by rotator evaporator. The residue was column chromatographed to give pale white colored solid products 1–2 in 89–90% yield.

Preparation of 2,2'-(ferrocenylmethylazanediyl)bis(N-benzylacetamide) (3). An analogous achiral compound 3 has been prepared by following a literature procedure[9a] and taken for further study.

(S,S-(-)-1). Yellow solid; MW 537. Yield: ca 478 mg, 89%. Melting point: 141°C. Anal. Calcd for [$C_{31}H_{35}FeN_3O_2$]: C, 69.27; H, 6.56; N, 7.82. Found: C, 69.51; H, 6.28; N, 7.65. ^1H NMR (400 MHz, $CDCl_3$) δ ppm: 7.28–7.35 (m, 10H, Ph); 6.84(s, 2H, -NHCO); 5.13(m, 2H,-CH); 4.07-4.54 (m, 9H, Fc); 3.52(s, 4H, -CH_2CO); 3.18 (2H, s, –CH_2 Fc); 1.42 (s, 6H, -CH_3). ^{13}C NMR (400 MHz, $CDCl_3$) δ ppm: 168.1, 143.1, 128.7, 127.4, 126.1, 69.9, 68.8, 58.2, 55.2, 48.5, 21.8.

R,R-(+)-2. Yellow solid; MW 537. Yield: ca 483 mg, 90%. Melting point: 142 °C. Anal. Calcd. for [$C_{31}H_{35}FeN_3O_2$]: C, 69.27; H, 6.56; N, 7.82. Found: C, 69.47; H, 6.65; N, 7.56. ^1H NMR (400 MHz, $CDCl_3$) δ ppm: 7.28–7.37 (m, 10H, Ph); 6.80(s, 2H, -NHCO); 5.12(m, 2H,-CH); 4.07–4.14 (m, 9H, Fc); 3.50(s, 4H, -CH_2CO); 3.16 (2H, s, –CH_2 Fc); 1.43 (s, 6H, -CH_3). ^{13}C NMR (400 MHz, $CDCl_3$) δ ppm: 168.1, 143.1, 128.7, 127.4, 126.1, 69.9, 68.6, 58.1, 55.1, 48.5, 21.8.

3. Yellow solid; MW 509. Yield: ca 462 mg, 87%. Melting point: 170 °C. Anal. Calcd. for [$C_{29}H_{31}FeN_3O_2$]: C, 68.37; H, 6.13; N, 8.25. Found: C, 68.51; H, 6.20; N, 8.38. ^1H NMR (400 MHz, $CDCl_3$) δ ppm: 7.62(s, 1H, -NHCO); 6.94(s, 1H, -NHCO); 7.22–7.37 (m, 10H, Ph); 4.45 (s, 4H, -CH_2NH); 4.07–4.38 (m, 9H, Fc); 3.51(s, 4H, -CH_2CO); 3.17 (s, 2H, –CH_2 Fc). ^{13}C NMR (400 MHz, $CDCl_3$) δ ppm: 170.1, 138.1, 128.7, 127.7, 127.5, 69.8, 68.6, 58.2, 55.1, 43.2, 30.9.

5. X-ray crystallography and data collection

Intensity data for 1-3 were collected on 'X-calibur, Eos, Gemini' X-ray diffractometer equipped with Eos CCD detector at 298 K for [$C_{62}H_{69}Fe_2N_6O_4$] 1, [$C_{62}H_{70}Fe_2N_6O_4$] 2 and [$C_{29}H_{31}FeN_3O_2$] 3 respectively. Monochromatic Cu-Kα X-ray (λ = 1.54184 Å for 1) and MoKα (λ = 0.71073 for 2 and 3) radiations were used for the measurements. Data was collected and reduced by using the ''CrysAlispro'' program (Version 1.171.37.33 Agilent Technologies, 2014) [24]. All the crystal structure were solved by the direct methods, and the refinement was carried out by full-matrix least squares against F^2 using SHELXL program package [25] and Olex2 (version 1.2.5) program package [26]. All non-hydrogen atoms were refined anisotropically.

Determination of IC_{50} for Enantiomers S,S-(-)-1 and R,R-(+)-2. MTT assay was performed to observe in vitro cytotoxicity of newly synthesized chiral tertiary amines S,S-(-)-1 and R,R-(+)-2 inhibitors holding biologically relevant ferrocene, amino-, and amidic- groups in the molecular Skelton. Carcinoma cell lines viz. Breast cancer cell line (MCF 7), Neuroblastoma cell line (IMR 32), Hepatocellular carcinoma cell line (HepG2) and immortal lung cell line (L132) were procured from the NCCS, Pune. Cells were cultured in required culture medium with supplementation of 10% FBS and incubated at 37 °C. For cytotoxicity determination, cells were seeded in 96 well plate (8000 cells per well) and incubated overnight for adhesion then treated by synthesized ligands for 24 h with five different concentrations. These cells were exposed to MTT solution (5 mg/ml) for 5 h at 37 °C. The formazon crystals, formed by mitochondrial activity of live cell, were dissolved in 200 μl of DMSO. Optical density was measured at 540 nm using plate reader. Percent inhibition due to exposure of synthesized enantiomers at each concentration was calculated and IC_{50} values (50% inhibition concentration) were derived. Metal based drug cisplatin was used as a reference .

Declaration of Competing Interest

The authors declare that they have no known competing financial interests or personal relationships that could have appeared to influence the work reported in this paper.

UNCORRECTED PROOF

Acknowledgements

VKS acknowledges CSIR New Delhi, India (Reference No. 01(2900)/17/EMR-II) and SERB-DST, New Delhi, India (Reference No. EMR/2016/003172) for the financial supports. We also thank the DST-PURSE and DST-FIST, New Delhi for the projects under which the single crystal X-ray diffractometer and NMR instruments were acquired in the Faculty of Science.

Supplementary materials

Supplementary material associated with this article can be found, in the online version, at doi:10.1016/j.jorganchem.2021.121983.

References

[1] R.A. Casero Jr., P.M. Woster, J. Med. Chem. 44 (2001) 1–26.
[2] N.P. Farrell, Chem. Soc. Rev. 44 (2015) 8773–8785.
[3] (a) G. Gasser I. Ott N. Metzler-Nolte J. Med. Chem. 54 2011 3 25 (b) C.G. Hartinger P.J. Dyson Chem. Soc. Rev. 38 2009 391 401 (c) G. Jaouen A. Vessieres S. Top Chem. Soc. Rev. 44 2015 8802 8817
[4] F. Bray, J. Ferlay, I. Soerjomataram, R.L. Siegel, L.A. Torre, A. Jemal, Cancer J. Clin. 68 (2018) 394–424.
[5] Y. Wang, H. Huang, Q. Zhang, P. Zhang, Dalton Trans 47 (2018) 4449–4454.
[6] (a) J.H. Kim A.R. Scialli Toxicol. Sci. 122 2011 1 6 (b) E.L. Izake J. Pharm. Sci. 96 2007 1659 1676
[7] (a) J.F. Vollano S. Al-Baker J.C. Dabrowiak J.E. Schurig J. Med. Chem. 30 1987 716 719 (b) F. Arnesano A. Pannunzio M. Coluccio G. Natile Coord. Chem. Rev. 284 2015 286 297
[8] D.L. Ma, M. Wang, C. Liu, X. Miao, T.S. Kang, C.H. Leung, Coord. Chem. Rev. 324 (2016) 90–105.
[9] (a) C.J. Savani H. Roy S.K. Verma D.R. Vennapu V.K. Singh Appl. Organomet. Chem. 35 2021 e6137 (b) D.R.V. Staveren N. Metzler-Nolte Chem. Rev. 104 2004 5931 5985 (c) A. Paul R. Borrelli H. Bouyanfif S. Gottis F. Sauvage ACS Omega 4 2019 14780 14789
[10] (a) G. Jaouen S. Top A. VessiEres G. Leclercq M. McGlinchey J. Curr. Med. Chem. 11 2004 2505 2517 (b) Q. Michard G. Jaouen A. Vessieres B.A. Bernard J. Inorg. Biochem. 102 2008 980 1985 (c) P. Pigeon S. Top O. Zekri E. A. Hillard A. Vessieres M.A. Plamont O. Buriez E. Labbe M. Huche S. Boutamine C. Amatore G. Jaouen J. Organomet. Chem. 694 2009 895 901
[11] B. Kater, A. Hunold, H.G. Schmalz, L. Kater, B. Bonitzki, P. Jesse, A. Prokop, J. Cancer Res. Clin. Oncol. 137 (2011) 639–649.
[12] R. Kadu, V.K. Singh, S.K. Verma, P. Raghavaiah, M.M. Shaikh, J. Mol. Struct. 1033 (2013) 298–311.
[13] R. Kadu, N.A. Wani, C. Savani, S. Aravinda, R. Rai, V.K. Singh, J. Mol. Struct. 1230 (2021) 129858.
[14] H. Helen, M. Paul, J. Elmar, M. Veldwijk, European Patent, No. EP 2 497 775 A1, 2012.
[15] (a) Y. Zhang K.T. Zhao S.G. Fox J. Kim D.R. Kirsch R.J. Ferrante R.I. Morimoto R.B. Silverman J. Med. Chem. 58 2015 5942 5949 (b) V.K. Singh R. Kadu H. Roy Eur. J. Med. Chem. 74 2014 552 561 (c) S. Luo P. Li S. Li Z. Du X. Hu Y. Fu Z. Zhang Mol. Pharm. 14 2017 1771 1781
[16] (a) S.N. Rao D.C. Mohan S. Adimurthy RSC Adv. 5 2015 95313 95317 (b) X. Peng Z. Sun P. Kuang L. Li J. Chen J. Chen Org. Lett. 22 2020 5789 5795
[17] V.K. Singh, R. Kadu, H. Roy, P. Raghavaiah, M.M. Shaikh, Dalton Trans 45 (2016) 1443–1454.
[18] E. Hillard, A. Vessieres, L. Thouin, G. Jaouen, C. Amatore, Angew. Chem. 118 (2006) 291–296.
[19] (a) J.R. Dimmock M.P. Padmanilyam G.A. Zello J.W. Quail E.O. Oloo J.S. Prisciak H.B. Kraatz A. Cherkasov J.S. Lee T.M. Allen C.L. Santos E.K. Manavathu E.D. Clercq J. Balzarini J.P. Stables Eur. J. Med. Chem. 37 2002 813 824 (b) J.R. Dimmock G.A. Zello E.O. Oloo J.W. Quail H.B. Kraatz P. Perjesi F. Aradi K. Takacs-Novak T.M. Allen C.L. Santos J. Balzarini E. D. Clercq J.P. Stables J. Med. Chem. 45 2002 3103 3111 (c) J.R. Dimmock M.P. Padmanilayam R.N. Puthucode A.J. Nazarali N.L. Motaganahalli G.A. Zello J.W. Quail E.O. Oloo H.B. Kraatz J.S. Prisciak T.M. Allen C.L.J. Santos E.D. Clercq E. K. Manavathu J. Med. Chem. 44 2001 586 593 (d) W.C.M. Duivenvoorden Y. Liu G. Schatte H. Kraatz Inorg. Chim. Acta. 358 2005 3183 3189
[20] C.J. Schlesener, C. Amatore, J.K. Kochi, J. Phys. Chem. 90 (1986) 3747–3756.
[21] A. Sacchi, A. Gasparri, C. Gallo-Stampino, S. Toma, F. Curnis, A. Corti, Clin. Cancer Res. 12 (2006) 175–182.
[22] R.A. Laskowski, B. M., J. Chem. Inf. Model. 10 (2011) 2778–2786.
[23] G. Zhang, S. Guo, H. Cui, J. Qi, Molecules 23 (2018) 524–528.
[24] CrysAlispro program (Version 1.171.37.33) Agilent Technologies, (2014).
[25] G.M. Sheldrick, Acta Cryst. C71 (2015) 3–8.
[26] (a) O.V. Dolomanov L.J. Bourhis R.J. Gildea J.A.K. Howard H. Puschmann J. Appl. Cryst. 42 2009 339 341 (b) L.J. Bourhis O.V. Dolomanov R.J. Gildea J.A. K. Howard H. Puschmann Acta Cryst A71 2015 59 75

UNCORRECTED PROOF